Medical Engineering and Physics 70 (2019) 9–18

Contents lists available at ScienceDirect

Medical Engineering and Physics

journal homepage: www.elsevier.com/locate/medengphy

A long-term mechanical cavopulmonary support device for patients with Fontan circulation

Marcus Granegger[a,b,e,*], Bente Thamsen[a,b], Emanuel J. Hubmann[a,b,d], Young Choi[a,b], Dominik Beck[a,b,d], Emanuela Valsangiacomo Buechel[b,c], Michael Voutat[b,c], Martin Schweiger[a,b], Mirko Meboldt[d], Michael Hübler[a,b]

[a] Pediatric Cardiovascular Surgery, Pediatric Heart Center, Department of Surgery, University Children's Hospital Zurich, Zurich, Switzerland
[b] Children's Research Center, University Children's Hospital Zurich, Zurich, Switzerland
[c] Pediatric Cardiology, Pediatric Heart Center, Department of Surgery, University Children's Hospital Zurich, Zurich, Switzerland
[d] pd|z Product Development Group Zurich, Department of Mechanical and Process Engineering, ETH Zurich, Zurich, Switzerland
[e] Biofluid Mechanics Laboratory, Institute for Imaging Science and Computational Modelling in Cardiovascular Medicine, Charité - Universitätsmedizin Berlin, Berlin, Germany

ARTICLE INFO

Article history:
Received 5 December 2018
Revised 15 June 2019
Accepted 19 June 2019

Keywords:
Single Ventricle Physiology
Cavopulmonary Assist Device
Blood Pump
Mechanical Circulatory Support
Computational Fluid Dynamics
3D Printing

ABSTRACT

In patients with a single ventricle, failure of the cardiovascular system may be prevented by substituting the missing sub-pulmonary ventricle with a pump. The aim of this study was to design and evaluate a device for long-term cavopulmonary support.

A radial pump with two inlets and two outlets, a single impeller, mechanical bearings, and dual motor configuration was developed. Motor and fluid dynamic components were designed and simulated using computational methods including thermal effects. Hydraulic properties were determined *in-vitro* with 3D-printed prototypes. The pump design was virtually implanted in an MRI-derived total cavopulmonary connection (TCPC).

Computational fluid dynamics (CFD) showed flow fields without regions of flow stagnation (velocity < 0.1 m/s) and only minor recirculations within the pump between 2–10 L/min against pressure heads of 0–50 mmHg at 2500–5000 rpm. The computed maximum temperature increase of blood due to motor heat was 1.3 K. Virtual implantation studies showed that the pump would introduce an additional volume of approximately 4 mL. Experimentally determined hydraulic performance results agreed well with CFD (deviation of <1.3 mmHg) and indicated pressure-sensitive characteristics ($\sim$-2.6 mmHg/(L/min)) while balancing the two inlet pressures ($\Delta P < 2.5$ mmHg) under imbalanced inflow conditions.

Through *in-silico* and *in-vitro* investigations, we demonstrated a promising pump design, which fulfills the basic requirements for long-term cavopulmonary support.

1. Introduction

In the USA and Europe, approximately 1% of all children are born with a congenital heart defect [1]. Approximately 8% of them suffer from an underdeveloped left or right ventricle [2]. There are two main treatment options for these patients: heart transplantation or the creation of the so-called "Fontan circulation" [3,4]. Whereas the availability of donor organs is limited, especially for children, the second option is palliative with reported long-term survival rates (25–30 years) ranging from less than 43 to 76% [5,6].

The formation of the Fontan circulation entails surgical connection of the caval veins directly to the pulmonary arteries without the interposition of a sub-pulmonary ventricle [7], creating the total cavopulmonary connection (TCPC). The body's venous return drains through the TCPC as it travels to the lungs (Fig. 1). Circumnavigation of the missing sub-pulmonary ventricle shifts the entire role of pumping blood to the single intact ventricle. This circulatory condition results in an inherently increased resistance to venous return; consequently, ventricular preload

Abbreviations: TCPC, total cavopulmonary connection; MCS, mechanical circulatory support; SVC, Superior vena cava; IVC, Inferior vena cava; RPA, Right pulmonary artery; LPA, Left pulmonary artery; CFD, Computational Fluid Dynamics.

* Corresponding author at: Biofluid Mechanics Laboratory, Institute for Imaging Science and Computational Modelling in Cardiovascular Medicine, Charité - Universitätsmedizin Berlin, Augustenburger Platz 1, 13353 Berlin, Germany.
E-mail address: marcus.granegger@charite.de (M. Granegger).

https://doi.org/10.1016/j.medengphy.2019.06.017
1350-4533/

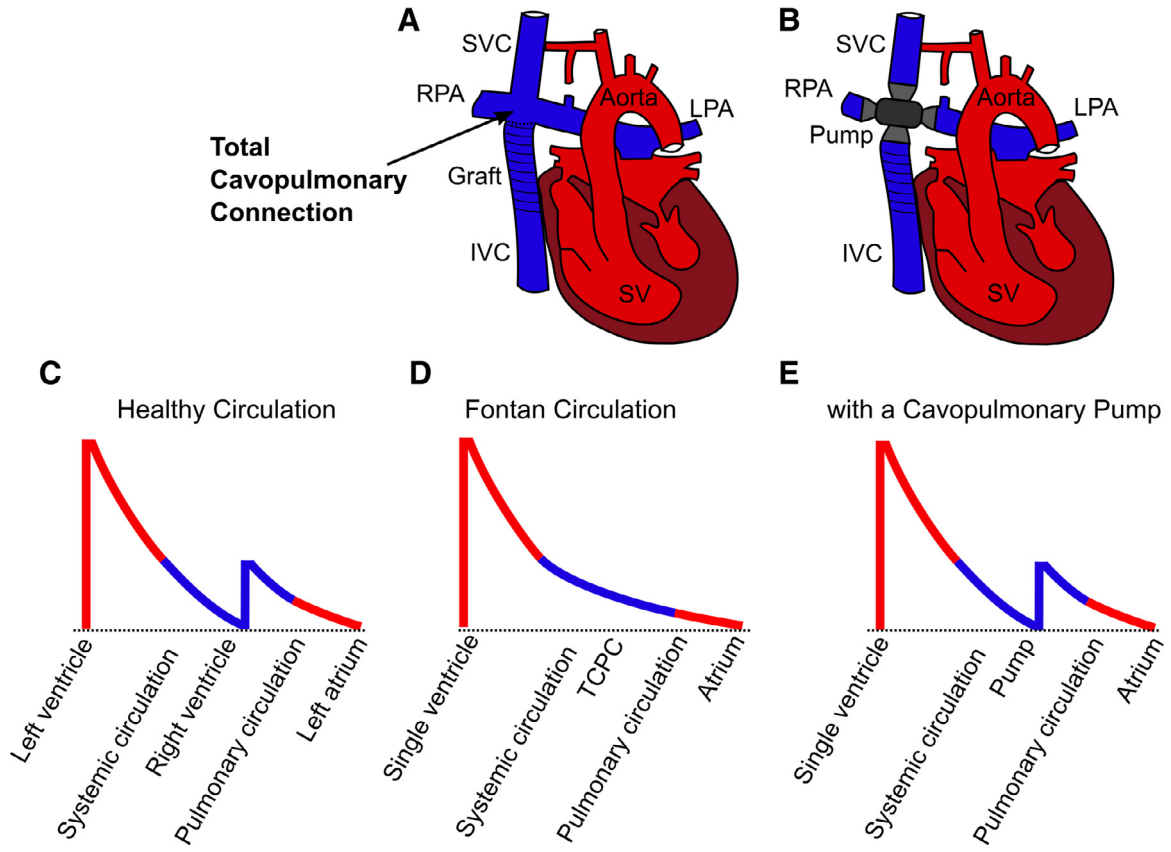

Fig. 1. (A): Anatomy of the heart and great vessels with a single ventricle circulation and a total cavopulmonary connection (TCPC) connecting the caval veins to the pulmonary arteries. (B): Implanted pump in cavopulmonary position. (C–E): Schematic representation of the pressure conditions in a healthy biventricular cardiovascular (CV) system, a univentricular CV system (Fontan) and the univentricular system supported by a pump. In the biventricular CV system, the right ventricle adds pressure to the venous blood before entering the lungs (C, blue line). In contrast, in the Fontan circulation the single ventricle comprises the only pressure source in the CV system leading to elevated venous pressures and lower systemic atrial pressure (D). With the introduction of a pump in cavopulmonary position, the pressures in the univentricular system could resemble those in the biventricular system (E). Figure adapted from Gewillig et al. [8]. SVC – Superior vena cava, IVC – Inferior vena cava, RPA - Right pulmonary artery, LPA – Left pulmonary artery, SV – Single ventricle, TCPC – Total cavopulmonary connection. (For interpretation of the references to color in this figure legend, the reader is referred to the web version of this article.)

and cardiac output are reduced with chronically elevated central venous pressure [8]. Although systemic oxygen saturation and volume overload issues are alleviated by the Fontan procedure, the overall cardiovascular system is often destined to fail in the second decade of life [3,8–11]: 20 years after Fontan completion only 70% of patients are free from failure [12]. Failure mechanisms range from ventricular dysfunction to deterioration of the Fontan circulation, which can be caused by an increase in pulmonary vascular resistance. Secondary symptoms to Fontan failure include venous congestion, lymphatic dysfunction, protein losing enteropathy, hepatic fibrosis, and plastic bronchitis [8].

Currently, the most accepted treatment option for failing Fontan patients remains the replacement of the heart with a healthy donor organ. In addition to the insufficient supply of donor hearts, heart transplantation in these patients is challenging and has a poorer outcome than in biventricular patients [13].

Mechanical circulatory support (MCS) potentially offers a promising treatment alternative, since it has already become the therapy of choice for adult patients with a biventricular circulation and end-stage heart failure [14]. Restoration of hemodynamic conditions similar to those of a normal biventricular system at an early point in the patient's life may be an effective treatment strategy for Fontan patients by stopping, or even reversing cardiovascular deterioration. This could be achieved by implantation of an MCS device specifically designed for the cavopulmonary location, pumping blood from the caval veins to the pulmonary arteries (Fig. 1A). Such a device could overcome the pulmonary vascular resistance (PVR) and restore pressure conditions to that of a normal biventricular circulation (Fig. 1C–E).

So far, the clinical application of MCS in Fontan patients is not state of the art, remains challenging, and only anecdotally reported [15–18]. Clinically available ventricular assist devices (VADs) have been adapted for cavopulmonary support as a bridge to transplantation [15,16]. Several other MCS concepts designed for cavopulmonary support have been proposed for the Fontan circulation in literature and are under investigation [19–26]. However, most of these reported approaches do not constitute an option for implantable long-term destination therapy for Fontan patients due to their design [21,27,28], or size and invasivity [15]. To our knowledge, only one radial pump, with two inlets and one outlet, has been tested in a first chronic animal experiment [29], indicating the potential of such a pump to permanently replace the right heart. All these efforts highlight the growing interest in the application and the persistent clinical need for a long-term treatment for the Fontan circulation.

Thus, we present a novel radial pump system for implantation in the TCPC that is specifically optimized to face the challenges of long-term cavopulmonary support: We introduce the defined requirements and present the mechanical, fluid dynamic, and electro-magnetic design. These components were analyzed regarding flow and temperature behavior *in-silico*. *In-vitro* verification of the hydraulic properties was performed employing rapid prototyping technologies.

2. Materials and methods

The conditions in the TCPC present specific design challenges, which differ from typical application of MCS as left ventricular assist devices (LVADs) [30].

We defined the requirements for long-term cavopulmonary support considering anatomic fit, surgical implantation, physiology, bearing and actuation components, hemocompatibility, as well as fluid design (Table 1) and developed our pump concept accordingly.

2.1. Pump mechanical design

The extravascular radial flow pump design constitutes a replacement for the missing sub-pulmonary ventricle to be used in young adolescent up to adult patients. It is a double-suction pump featuring two in- and two outlets, and a single impeller suspended between two mechanical bearings (Fig. 2). The mechanical ball-cup bearings that fix the impeller position between two flow straighteners at the inlets are similar to those used in the clinically established Heartmate II rotary blood pump (Abbott Inc, Chicago, Illinois, USA) [34], permitting a small pump size and large fluid gaps for secondary flows.

The impeller has a diameter of 19 mm and four curved blades, two short and two long ones which are connected to the central hub. Wide gaps of 0.5 mm between the rotating impeller shrouds and the static upper and lower housing walls were incorporated. This permits good washout of the secondary flow channels which on the one hand ensures cooling of the adjacent motor coils and on the other hand prevents pump thrombosis. A ring chamber is used as the outlet casing design. In contrast to volute casings, ring chambers have a broader operating range with stable characteristics [35], thus allowing for a larger range of flow rates and pressure heads, which was a design requirement for our cavopulmonary pump.

To address the requirement of a small pump size to accommodate implantation in young adolescent patients, virtual fitting of the pump design in an exemplary TCPC case was performed. Following institutional review board approval, MRI images of a TCPC from an 11-year-old Fontan patient were reconstructed using Mimics software (Materialise NV, Leuven, Belgium). Siemens NX computer-aided design (CAD) software (Siemens PLM Software, Plano, Texas, USA) was used to globally add a 0.75 mm vessel thickness to the reconstructed fluid geometry to mimic the vessel walls and to virtually implant the pump. After volumetric measurement of the TCPC junction, it was virtually replaced by the pump by at-

Table 1
Major requirements for a pump in cavopulmonary position.

Anatomic and Surgical Aspects	➢ Versatility for a large variety of TCPC geometries: Implantation in a wide Fontan patient group is envisaged. ➢ Small device volume: Compression of surrounding structures such as bronchi and pulmonary veins must be prevented. ➢ In- and outflow configuration design featuring no unnecessary angles to prevent graft kinking. ➢ Low implantation complexity.
Physiology	➢ Wide operating range to support the patient during rest (as low as 2 L/min) and during physical activity (up to 10 L/min) and allow for physiologic control [31]. ➢ Well mixed hepatic flow distribution to left and right PA to prevent pulmonary arteriovenous malformations [32]. ➢ Intrinsic balancing of pressures in IVC and SVC to facilitate physiologic venous return mechanisms even in case of unbalanced inflow conditions (3:1) [33]. ➢ Pressure sensitive pump characteristics: Slope of the HQ curve should be higher than -5 mmHg ·min/L to permit sufficient adaptation to altered pressure conditions [31].
Hemocompatibility	➢ Resistance against thrombi: Wide flow gaps ($\geq$ 0.5 mm) allow floating thrombi to pass the pump. ➢ Good washout: No regions with low velocities and excessive recirculation to prevent thrombus formation. ➢ Smooth interface between pump and vasculature: No unnecessary angles and steps to prevent flow detachment and consequent thrombus formation. ➢ Low blood trauma potential: Shear rates should be lower than in currently available rotary blood pumps.
Actuation and Bearing	➢ Failsafe: Redundant motor design to prevent pump stops. ➢ Robust against venous vasculature collapse: Bearing must cope with forces during suction events. ➢ Low mechanical wear: Wear of all components must allow an operation of >10 years. ➢ No critical blood temperature with a maximum temperature increase of 2 K. ➢ Low power consumption to permit extended battery life.

TCPC - total cavopulmonary connection, PA - pulmonary arteries, IVC - inferior vena cava, SVC - superior vena cava.

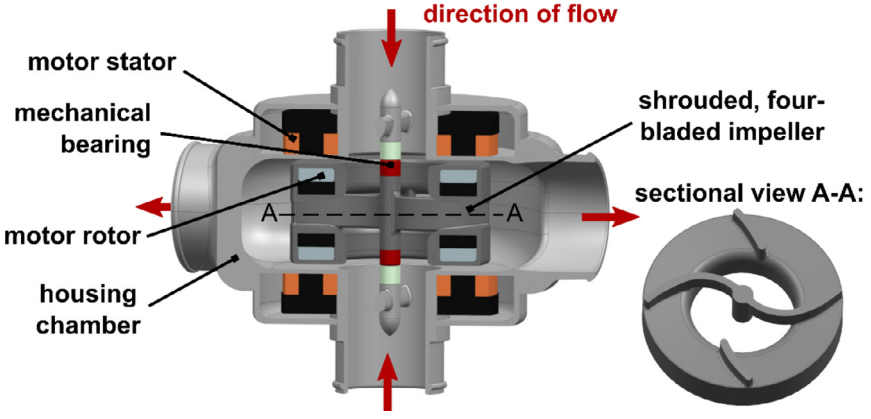

Fig. 2. Computer aided design model of the cavopulmonary pump concept. Left: Sectioned internal component view with the indicated blood flow direction. Right: Detailed sectional view of the impeller with four blades, two longer ones connected to the central hub.

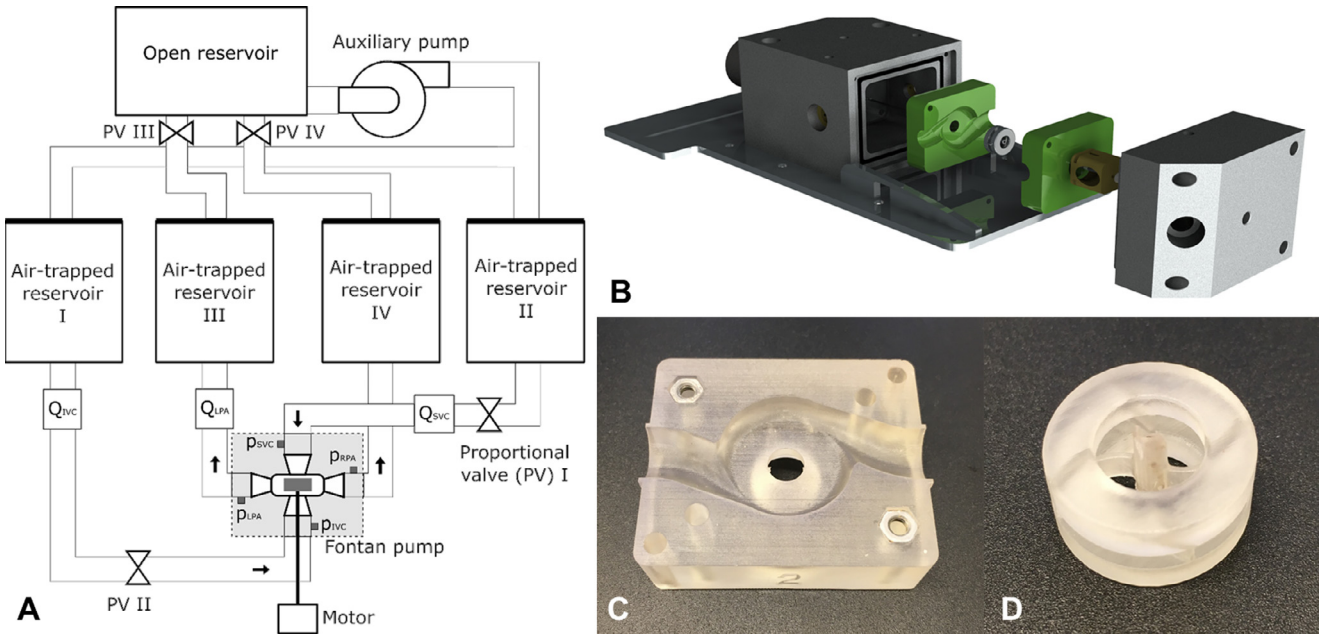

Fig. 3. (A): Schematic of the *in-vitro* mock circulation used to measure the hydraulic performance. (B): Exploded computer aided design (CAD) assembly view of the custom-made modular housing unit used for hydraulic experiments; the pump housing and the impeller, which was loaded onto the central drive shaft driven by an exterior motor is exhibited. (C): 3D-printed pump housing, (D): 3D-printed pump impeller.

taching grafts to the vessels. The additional volume introduced by the implantation of the pump was calculated.

2.2. Hydraulic pump characteristics

Firstly, we aimed for a flat pressure-flow relationship (H-Q curve, Fig. 5) [36], to allow intrinsic adaptation of the pump output to changes in venous return at constant speeds. Flat hydraulic characteristics are even more imperative without a physiologic control mechanism for automated speed adaptation of the pump [31]. Secondly, we aimed to design a pump that mimics the pressure conditions in the right atrium: in healthy individuals, the inferior vena cava (IVC) and superior vena cava (SVC) drain into the right atrium and consequently against the same pressure. Therefore, even in the case of highly imbalanced IVC/SVC flows, the pressures proximal to the pump for the SVC and IVC should be nearly equivalent to ensure physiologic perfusion of the upper and lower body remains undisrupted.

Thirdly, we aimed for a hydraulic pump design with adequate hemocompatibility so that risks for pump thrombosis, as well as blood trauma and activation of corpuscular blood components are minimized. It is well known that these effects are related to the local flow conditions: thrombosis is associated with stagnant and recirculating flow [37], and blood trauma and activating effects are caused by high shear stresses in the blood flow [38]. Adequate washout to cool the bearing, which generates heat due to friction, must be provided. Good washout was determined by the absence of flow stagnation, defined by blood velocities greater than 0.1 m/s adjacent to the bearings.

The hydraulic performance of the pump with regard to these requirements was experimentally and numerically investigated.

2.2.1. Experimental analysis

Hydraulic performance was evaluated using a mock circulation with two inlets and two outlets and four reservoirs to simulate the TCPC junction (Fig. 3). Flows were measured using clamp-on flow sensors (Sonoflow CO.55, Sonotec, Halle, Germany) and automatically controlled with solenoid valves (TFM15-B2-C, Tsai Fan, China). Automated control was implemented by a real-time control system (Microlabbox, dSpace, Paderborn, Germany). Pressures were measured using fluid-filled pressure transducers (APT300, Harvard Apparatus, Holliston, MA, USA). The fluid geometry was modelled using 3D-printed prototypes (Form 2, Formlabs Inc., Somerville, USA) (Fig. 3C–D) and loaded into a custom-made sealed housing unit (Fig. 3B) with a central drive shaft passing through the rotor driven by an exterior motor (DC Motor EC32, Maxon Motor, Sachseln, Switzerland).

A water/glycerine mixture was used to model blood and monitored using a real-time viscosity sensor (DEVIL, Avenisense, Le Bourget-du-Lac, France) to maintain a viscosity of 3.0 – 3.5 mPa·s. The overall pump pressure head for H-Q curves was calculated as the difference between the average outlet pressures and the average inlet pressures. H-Q curves and differences between the inlet pressures ($\Delta P = P_{IVC} - P_{SVC}$) were measured at three different pump speeds (2200, 2500, 2800 rpm) over a range of flow rates (0–7.5 L/min) with three different inlet flow distributions (SVC:IVC 1:1, 1:2, 1:3). The pressure drop across the pump with the motor stopped and impeller stalled was measured with the three different inflow ratios as well.

2.2.2. Numerical analysis

Fluid dynamic and hydraulic performance characteristics of the pump were calculated and analyzed by employing computational fluid dynamics (CFD) [39] using Star CCM+ software (Siemens, Munich, Germany) such as in [40]. Ten operating points at flow rates from 2 to 10 L/min, inlet flow ratios between SVC and IVC from 1:1 to 1:3, and rotational speeds from 2500 to 5500 rpm were simulated. Focus was laid on the most clinically relevant operating conditions at a constant rotational speed of 2500 rpm: 1) a condition simulating the typical Fontan flows of a young adolescent patient with a total flow rate of 4 L/min and an inflow ratio between SVC and IVC of 1:2 [41], 2) a condition simulating the effect of a low flow rate of 2 L/min with inflow ratios of 1:1 and 1:2, and 3) a condition simulating slight physical activity with a higher flow rate of 6 L/min with inflow ratios of 1:2 and 1:3. To investigate extreme conditions in terms of the thermal effects due to increased mo-

tor losses, we also investigated higher speeds (3500 to 5500 rpm) at a high flow rate of 10 L/min. Details regarding the applied CFD methodology are presented in the supplementary material.

Results from the CFD studies were assessed regarding hydraulic performance and overall flow structures. To evaluate blood damage potential, viscous shear stresses (vss) and wall shear stresses (wss) were calculated based on flow fields that were averaged over one rotation.

Temperature increase of blood due to motor losses was determined by simulation of convective heat transfer, which is the transfer of thermal energy from a surface to an adjacent moving fluid. The approach accounted for advection as well as diffusion and was based on Newton's law of cooling:

$$q = h \cdot \left(T_{surface} - T_{fluid}\right) \tag{1}$$

where q is the local surface heat flux in W/m^2, h is the local convective heat transfer coefficient in W/(m^2·K), and T is the temperature of the surface/fluid in K. This phenomenon was implemented by setting heat sources corresponding to the predicted motor losses (Section C, Fig. 7) on both sides of the top and bottom housing surface in contact with blood that is adherent to the motor stator as a boundary condition. The heat transfer coefficient was simulated with CFD based on thermal fluid properties [42] that were set for blood as a specific heat of 3650 J/kg/K and a thermal conductivity of 0.5 W/m/K [43]. Thermal effects were critically evaluated at simulated worst-case scenarios: 1) when motor losses are at their maximum, or 2) when gap washout was simultaneously expected to be reduced due to lower pump pressure heads.

To evaluate the fluid dynamic and mechanical boundary conditions for the bearing, analysis of the flow structures adjacent to the mechanical bearing and determination of the axial and radial forces acting on the impeller was carried out with CFD.

2.3. Actuation design

The actuation system comprises two axial flux three-phase synchronous motors each having concentrated stator windings with 12 coils and one rotor with 8 poles of surface-mounted permanent magnets. For the design of the actuation, we combined CFD, electromagnetic simulations, and analytical approaches. The torque demand $T_{impeller}$ (Nm) for the actuation and the resulting hydraulic pump efficiency η (-) as in Eq. (2)

$$\eta(H, Q) = 133.322 \cdot H \cdot 10^{-3}/60 \cdot Q \cdot \left(2\pi f/60 \cdot T_{impeller}\right)^{-1} \tag{2}$$

was determined using CFD results for static pressure head H (mmHg), flow rate Q (L/min), rotational speed f (rpm), and impeller torque $T_{impeller}$ (Nm) (Table S1). The detailed derivation of the conducted hydraulic efficiency interpolation over the entire operating range is presented in detail in the supplementary material. The peak linked magnetic flux $\hat{\Psi}$ (Wb) by one motor phase was computed with computational electromagnetics within a 3D finite element method simulation (ANSYS Electronics Desktop, ANSYS Inc., Canonsburg, USA). The torque constant k_T (Nm/A) for each of the motors was determined as:

$$k_T := \frac{T_{el}}{I_{ph,RMS}} = \frac{3p}{\sqrt{2}}\hat{\Psi} \tag{3}$$

where p is the number of pole pairs and $I_{ph,RMS}$ the root mean square (RMS) of the phase current.

In the final implant, medical grade titanium (Titanium Grade 5 ELI) is envisaged as impeller and housing material. The eddy-current loss in the housing and stator core losses for soft magnetic composite material (SOMALOY™ 500) were approximated as previously reported [44,45]. The heat losses per motor P_{loss} (W) were determined for all operating conditions with MATLAB (The MathWorks Inc., Natick, USA). Copper losses assuming a winding copper fill factor of 0.43 were taken into account as well as non-copper losses, which were considered as a rotational speed f (rpm) dependent break torque (T_L):

$$P_{loss} = \frac{3 \cdot R_{ph}}{{k_T}^2}\left[T_{impeller}(f, Q)/2 + T_L(f)\right]^2 + T_L(f)2\pi f/60 \tag{4}$$

where R_{ph} (Ω) is the phase resistance and $T_{impeller}$ (Nm) is the delivered torque of both motors combined. Resulting losses per motor P_{loss} were used as an input for CFD simulations to subsequently determine the maximum increase of blood temperature in the aforementioned worst-case scenarios.

3. Results

3.1. Pump mechanical design

Excluding the in- and outlets, the maximum diameter of the pump housing is approximately 30 mm and the maximum height approximately 19 mm. The inlets and outlets are designed as connectors with end internal diameters of 11 and 12 mm, respectively, to permit the attachment of prosthetic grafts. We envisage the use of conical grafts, which will be anastomosed to the corresponding vessels, facilitating implantation of the device in children as young as 10 years old [46].

The virtually implanted pump in an 11-year-old patient's Fontan TCPC is depicted in Fig. 4. The extra volume contributed by the addition of the pump was approximately 4 mL. In order to permit fitting of the pump at the TCPC, the SVC and IVC were laterally translated by less than 10 mm.

3.2. Hydraulic pump performance

3.2.1. Experimental results

The experimentally measured H-Q curves indicate a pressure sensitive behavior with average slopes ranging from −2.3 to −2.9 mmHg/(L/min) for relevant clinical operating ranges at three pump speeds (2200, 2500, 2800 rpm) and three inflow ratios (1:1, 1:2, 1:3) as shown in Fig. 5.

Pump performance was not noticeably affected by imbalanced inflow ratios as shown by close agreement of the corresponding imbalanced inflow H-Q curves for each pump speed (Fig. 5A). The two large entry openings of the impeller at the junction where the two inflow paths meet promoted balancing of inlet pressures: The maximum pressure difference between the two inlets was 2.5 mmHg with an inflow distribution of 2 and 6 L/min (Fig. 5E). The pressure drops across the stopped pump ranged from 0.9 to 6.0 mmHg and resistances of 1.0 to 2.4 mmHg/(L/min) for flows from 2 to 5 L/min.

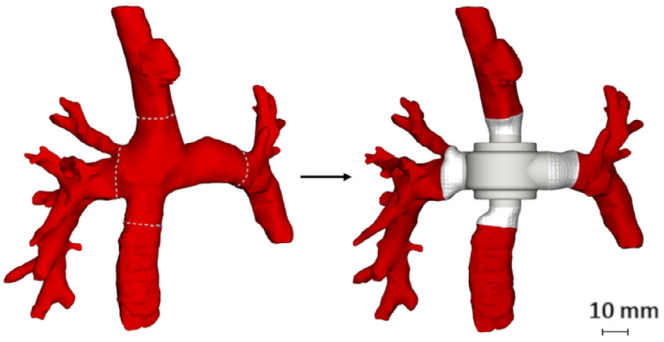

Fig. 4. Original Fontan TCPC of an 11-year-old patient with dashed lines depicting the section that was removed for placement of the pump (left). Virtual implant of pump with conical prosthetic grafts connected to the in- and outlets, attaching the pump to the corresponding vessels (right). TCPC - total cavopulmonary connection.

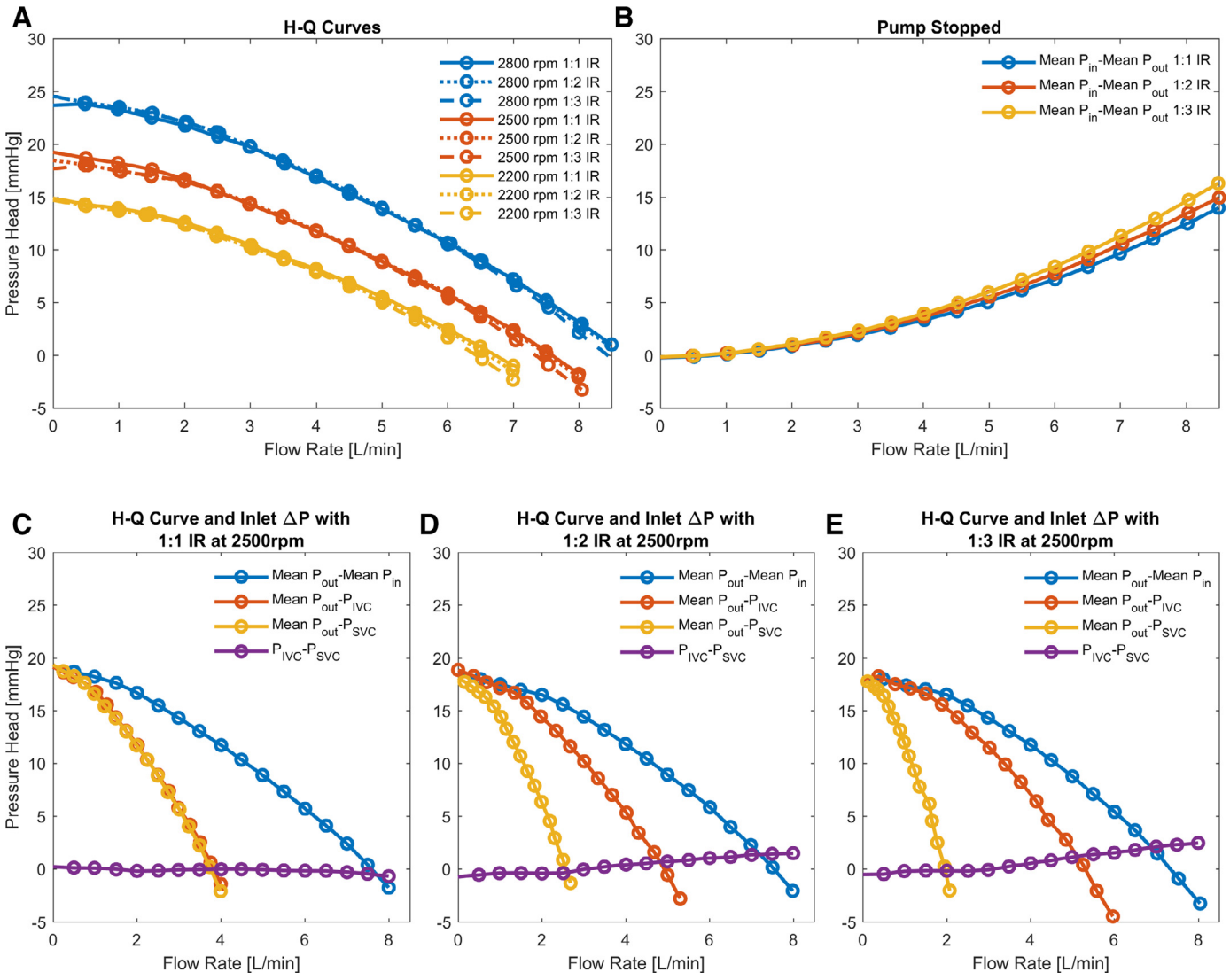

Fig. 5. (A): Experimentally measured H-Q curves at three different rotational speeds with three different inflow ratios (IRs). (B): Pressure drop across the pump when the pump rotor is stopped with three different IRs. (C): H-Q curve at 2500 rpm, the H-Q contributions from the IVC and SVC, and inlet ΔP ($P_{IVC} - P_{SVC}$) curve during a balanced 1:1 IR, (D): imbalanced 1:2 IR, and E: imbalanced 1:3 IR. IR - inflow ratio, IVC – Inferior vena cava, SVC – Superior vena cava.

3.2.2. Numerical results

In the main operating condition, with a flow rate of 4 L/min and an inflow ratio between SVC and IVC of 1:2, the pump reached a mean pressure head of 11.3 mmHg at a hydraulic efficiency of 40%. The CFD calculated hydraulic performance results over the clinically relevant operating range are presented in detail in the supplementary material (Table S1). The CFD gained results agreed well with the measured ones with a maximum deviation of 1.3 mmHg. The washout of secondary flow channels between the impeller shrouds and the housing was calculated as the averaged flow rate through the axial gaps, which was between 416 and 595 mL/min. The highest washout occurred for the lowest overall flow rate at its respective high pressure head. Blood volumes affected by shear stresses of more than 9, 50, and 150 Pa were $<$1 mL, $<$0.01 mL, and $<$0.0001 mL, respectively. The largest volumes occurred at the highest flow rate at 6 L/min in the most imbalanced condition (1:3 inflow ratio).

The velocity fields and the wall shear stresses on the internal structures are displayed in Fig. 6. Flow fields did not show prominent detachments zones within the blade channels, gaps, and ring chamber. Larger recirculation zones only developed in the outlet channels at lower flow rates.

With regard to washout of the bearing regions, all investigated conditions indicated a smooth flow without low or stagnating velocities around the bearing sites, leading to wall shear stresses above 1 Pa [37].

Maximum fluid-dynamic axial forces on the bearings were computed to be in the range between 40 mN (in a balanced low flow condition at 2 L/min and 2500 rpm) and 150 mN (in an unbalanced high flow condition at 10 L/min and 5500 rpm). Mean radial forces were generally balanced and below peak values of 80 mN in the investigated operation range.

3.3. Actuation

The motors cover the entire range of operating conditions for young adolescents and adults from less than 2 L/min to more than 10 L/min with speeds from 1800 to 5500 rpm.

Fig. 7 (left) depicts the hydraulic model (H-Q curves (Eq. S4)) together with the predicted heat losses on one housing side from

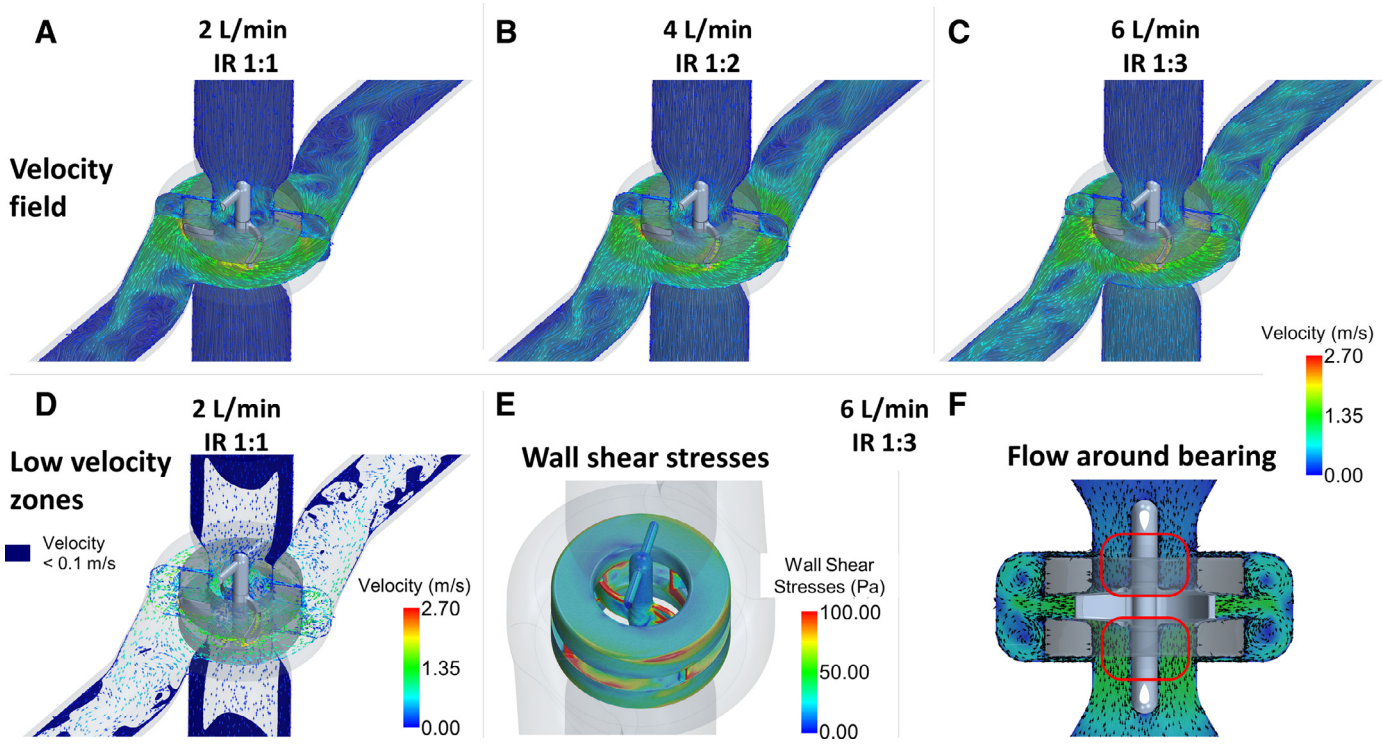

Fig. 6. Computational Fluid Dynamics simulated flow fields at the clinically most relevant speed of 2500 rpm for three different flow rates and inflow ratios (IR). (A–C): velocity fields plotted as line Integral convolution with superimposed velocity vectors on two cut planes parallel to the pump's inlets and outlets revealed overall smooth flow structures within the pump: No prominent recirculation or stagnation zones developed within the pump. At lower flow rates, low velocities were observed within the outlet channels. Second row: (D): Low velocity zones (velocities < 0.1 m/s) displayed in dark blue for the 2 L/min case. Stagnating flow is only seen within the inlet and outlet channels. E: Wall shear stresses on the impeller, flow straightener, bearing and central hub for the 6 L/min case. Highest wall shear stresses occur at the blade and shroud edges. (F): The flow around the mechanical bearings is shown by the velocity field for the 6 L/min case. Streamlined flow around the bearing sites can be observed. In fact, the secondary flow through the upper and lower axial gap entering the main flow restricts the pump inlet cross-sectional area thereby generating streamlined flow with higher velocities around the central hub and bearing sites, as depicted in the lower right panel. (For interpretation of the references to color in this figure legend, the reader is referred to the web version of this article.)

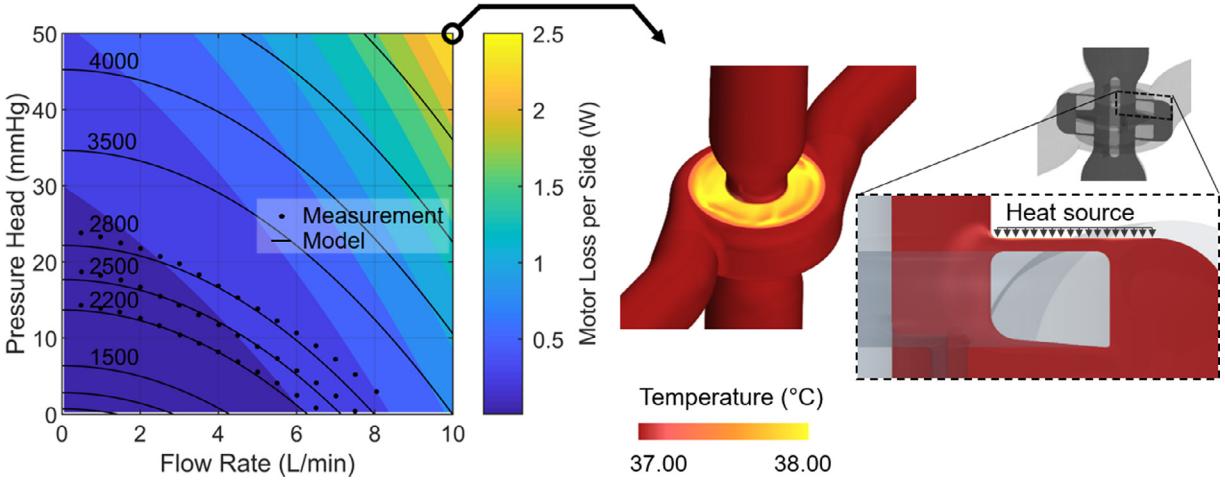

Fig. 7. Left: Modelled (solid lines) and measured H-Q curves (dots) over the entire operating range of the pump with expected heat losses per motor. Right: Computational fluid dynamics simulated temperature distribution directly at the housing wall and within the axial gap between the rotor and housing at 5500 rpm and 10 L/min corresponding to maximum motor losses.

one single motor over the entire expected operating range. Within this operating range, the maximum losses per motor were less than 3 W.

CFD derived blood temperatures increased proximal to the motor less than 1.5 K in all investigated operating conditions. Motor losses increased with higher rotational speeds and higher flow rates (Fig. 7). We found the worst-case scenario to be, when motor losses are at their maximum (highest rpm and flow rate) at 5500 rpm at 10 L/min. A heat source of 2.6 W on both housing sides adjacent to a motor resulted in maximum local blood temperatures of 38.4 °C (Fig. 7, right).

4. Discussion

In this study, we present a pump for support in cavopulmonary position with potential for long-term application in young ado-

lescents up to adult patients with a Fontan circulation. Functioning as a surrogate for the sub-pulmonary ventricle, the proposed pump may reduce venous congestion, improve ventricular preload and may thereby stop or even prevent the natural deterioration of the Fontan circulation before potentially irreversible cardiovascular remodeling, such as liver cirrhosis [47], takes place. The pump could be specifically effective in patients with preserved ventricular function since the heart could adapt to the hemodynamic changes evoked by the pump, whereas in patients with an already failing ventricle, the increase in cardiac output generated by the pump may be detrimental. The remaining uncertainty surrounding the physiological ramifications for such a pump necessitates future investigations into the phenotypes of Fontan patients that could benefit most from such a therapy using appropriate *in-vivo* models.

Several groups have previously demonstrated feasibility of MCS devices for Fontan failure. Unlike other pump concepts that only contribute a small pressure head [48], but similar to the concept of Csysk et al. [29], the proposed pump concept is designed to deliver the physiological range of sub-pulmonary ventricular flows from 2 to more than 10 L/min against pressure heads of up to 50 mmHg. By incorporating a previously described physiological control algorithm that adapts the pump speed based on the pressure difference between the pump inlet and the systemic atrium [31], a wide range of hemodynamic augmentation adaptable to the patient's needs is granted extending from rest to physical activity.

Another potential hemodynamic advantage of our proposed pump is its capability to imitate the right atrium by balancing inlet pressures for the SVC/IVC. Even in cases of drastically imbalanced venous returns from the IVC and SVC, which may particularly occur during physical activity, the pressure difference was less than 2.5 mmHg. Other pump concepts have not demonstrated similar capabilities. Furthermore, some concepts aim to support the IVC only [21] which increases pulmonary artery and SVC pressures at the same magnitude; thus, possibly compromising normal venous return mechanisms [49].

Besides fulfilling the hemodynamic requirements, a long-term device for Fontan patients must perform superbly in terms of blood trauma and thrombosis. We designed wide gaps with a minimum clearance of 0.5 mm and exhibited favorable fluid dynamic properties over a wide range of operating conditions by a well-guided flow. Forgiving flow structures such as the ring chamber, instead of a design-point optimized volute casing, allow for a wide operating range. Shear stresses were predicted to be much lower than in common radial blood pumps (volumes exposed to scalar shear stress >150 Pa are less than 0.003% of values published for clinical VADs [50]), suggesting a low blood trauma profile of our MCS device for cavopulmonary support.

Regarding thrombosis risk, CFD showed good washout characteristics within the pump void of major recirculation and stagnation zones as well as augmented flow rate through the wide secondary flow channels. From the recent clinical experience with the HeartMate 3 [51], it can be deduced that wide flow channels, considerably larger than typical hydrodynamic bearings, may prevent pump thrombosis, possibly by allowing for thrombi to pass through the pump instead of being trapped inside the device [52]. The resistivity against pump thrombosis of our pump may thus be superior compared to pumps designed for cavopulmonary support with small hydrodynamic bearing gaps [29].

The good washout of the axial gaps is a further advantage regarding temperature generation due to motor heat losses, which may be major contributors to poor hemocompatibility of a blood pump. Due to the small pressure head of the main operating conditions of a Fontan pump (5–15 mmHg) compared to that of usual blood pumps (45–100 mmHg), delivering sufficient backflow in the gaps between impeller and housing is generally harder to achieve. In the proposed system, an acceptable temperature increase was observed.

An important contributor to hemocompatibility and pump performance is the bearing. Design considerations for mechanical bearings in blood pumps include acceptable wear [34] and a well-washed design [53] to minimize the risk of heat and thrombi generation. In the proposed pump design, bearing structures are placed further from the impeller inlet regions so that the flow field around the bearing could be smoother than in other blood pumps [54]. Furthermore, axial forces during regular operation are considerably lower than those for LVADs because of low pressure heads across the pump and the symmetric design between opposite inlets and outlets. Heat generation in the bearing is thus expected to be drastically lower than in conventional LVADs.

Despite the promising characteristics in terms of hemodynamics and hemocompatibility, placement of the pump in the TCPC junction presents a high risk for the patient in the case of device failure. We showed that in the scenario of a stopped pump impeller, the resistance of the pump is in the same range as the PVR and similar to previously presented results of other pumps with similar application [25]. It remains open to debate whether such a hydraulic resistance is acceptable. However, the HeartMate 3 experience indicated that reliability of implantable rotary blood pumps can be high with low rates of pump replacements due to device malfunction (1.6%, [55]), implying that a pump stop can be considered a rare event.

A disadvantage compared to intravascular pumps [19] is the required invasive implantation procedure. Implantation of the pump is challenging due to the limited anatomical space around the TCPC, proximity of sensitive structures such as the bronchus and pulmonary veins, and additional surgical complexity associated with operating on the typical Fontan patient with multiple previous surgeries. Since the proposed pump is smaller than other concepts [29] and replaces the volume originally occupied by the TCPC junction, the amount of additionally implanted volume by the pump and graft material is small. With the option for variably-sized graft attachments, we would expect our system to be able to treat a large number of Fontan patients despite heterogeneous TCPC anatomies. Nevertheless, implantation of such a device remains challenging and innovative surgical procedures may be required.

In conclusion, a novel small extravascular pump for circulatory assistance in Fontan patients was investigated *in-silico* and *in-vitro*. In addition to demonstrating its capability to maintain normal physiologic hemodynamics, our pump design showed low shear rates, good washout, and thus potentially good hemocompatibility; therefore, it may represent promising design aspects for mitigating the typical adverse events associated with current MCS devices. The pump is intended for implantation for long-term use in cavopulmonary location for a large proportion of Fontan patients, starting from young adolescents to adults.

The presented study has a number of limitations. In the computational method, we assumed steady boundary conditions. The approach to simulate heat transfer assumes a linear relationship between heat flux and temperature difference of media and further relies on standard wall functions from turbulence modelling for calculating the near wall boundary layer, which could not be validated within the frame of this study.

The derivation of motor losses is based on a combined *in-silico* and analytical approach. The pump hydraulic efficiency extrapolation (Eq. S3) was simplified with parabolic curves [56]. Additional losses due to friction in the mechanical bearings are expected to be small and thus regarded to be negligible. For the thermal assessment, it was conservatively assumed that the motor heat is not spread over the whole pump housing, and no heat is transferred

to the surrounding tissue. An experimental validation of this approach was beyond the scope of this work.

Acknowledgments

The authors gratefully acknowledge the financial support by the UZH Foundation. This work is part of the FontanAssist branch of the Zurich Heart project under the umbrella of "University Medicine Zurich".

Ethical approval

Patient data were collected with informed consent and the study was approved by the Swiss Ethics Committees on research involving humans (ID 2017-00566).

Competing interests

None declared.

Funding

As stated in the acknowledgements at the end of the manuscript.

Supplementary material

Supplementary material associated with this article can be found, in the online version, at doi:10.1016/j.medengphy.2019.06.017.

References

[1] Triedman JK, Newburger JW. Trends in congenital heart disease. Circulation 2016;133:2716–33. doi:10.1161/CIRCULATIONAHA.116.023544.
[2] O'Leary PW. Prevalence, clinical presentation and natural history of patients with single ventricle. Prog Pediatr Cardiol 2002;16:31–8. doi:10.1016/S1058-9813(02)00042-5.
[3] Goldberg DJ, Shaddy RE, Rivashankar C, Rychik J. The failing Fontan: etiology, diagnosis and management. Expert Rev Cardiovasc Ther 2011;9:785–93. doi:10.1586/ERC.11.75.
[4] Gewillig M. The Fontan circulation. Heart 2005;91:839–46. doi:10.1136/hrt.2004.051789.
[5] Pundi KN, Johnson JN, Dearani JA, Pundi KN, Li Z, Hinck CA, et al. 40-Year Follow-Up after the Fontan operation long-term outcomes of 1,052 patients. J Am Coll Cardiol 2015;66:1700–10. doi:10.1016/j.jacc.2015.07.065.
[6] D'udekem Y, Iyengar AJ, Galati JC, Forsdick V, Weintraub RG, Wheaton GR, et al. Redefining expectations of long- Term survival after the Fontan procedure twenty-five years of follow-up from the entire population of australia and new zealand. Circulation 2014;130:S32–8. doi:10.1161/CIRCULATIONAHA.113.007764.
[7] Gewillig M, Brown SC. The Fontan circulation after 45 years: update in physiology. Heart 2016;102:1081–6. doi:10.1136/heartjnl-2015-307467.
[8] Gewillig M, Goldberg DJ. Failure of the Fontan circulation. Heart Fail Clin 2014;10:105–16. doi:10.1016/j.hfc.2013.09.010.
[9] Earing MG, Cetta F, Driscoll DJ, Mair DD, Hodge DO, Dearani JA, et al. Long-term results of the Fontan operation for double-inlet left ventricle. Am J Cardiol 2005;96:291–8. doi:10.1016/j.amjcard.2005.03.061.
[10] Khairy P, Fernandes SM, Mayer JE, Triedman JK, Walsh EP, Lock JE, et al. Long-term survival, modes of death, and predictors of mortality in patients with Fontan surgery. Circulation 2008;117:85–92. doi:10.1161/CIRCULATIONAHA.107.738559.
[11] Atz AM, Zak V, Mahony L, Uzark K, D'agincourt N, Goldberg DJ, et al. Longitudinal outcomes of patients with single ventricle after the Fontan procedure. J Am Coll Cardiol 2017;69:2735–44. doi:10.1016/j.jacc.2017.03.582.
[12] d'Udekem Y, Iyengar AJ, Cochrane AD, Grigg LE, Ramsay JM, Wheaton GR, et al. The Fontan procedure: contemporary techniques have improved long-term outcomes. Circulation 2007;116:I157–64. doi:10.1161/CIRCULATIONAHA.106.676445.
[13] Kirklin JK, Pearce FB, Dabal RJ, Jr WFC, Mauchley DC. Challenges of cardiac transplantation following the Fontan procedure. In: Proceedings of the fifth science meeting of the world society for pediatric and congenital heart surgery, 8; 2017. p. 480–6. doi:10.1177/2150135117714460.
[14] Ponikowski P, Voors AA, Anker SD, Bueno H, Cleland JGF, Coats AJS, et al. 2016 ESC guidelines for the diagnosis and treatment of acute and chronic heart failure: the task force for the diagnosis and treatment of acute and chronic heart failure of the european society of cardiology (ESC). Developed with the special contribution. Eur J Heart Fail 2016;18:891–975. doi:10.1002/ejhf.592.
[15] Prêtre R, Häussler A, Bettex D, Genoni M. Right-Sided univentricular cardiac assistance in a failing Fontan circulation. Ann Thorac Surg 2008;86:1018–20. doi:10.1016/j.athoracsur.2008.03.003.
[16] Valeske K, Yerebakan C, Mueller M, Akintuerk H. Urgent implantation of the berlin heart excor biventricular assist device as a total artificial heart in a patient with single ventricle circulation. J Thorac Cardiovasc Surg 2014;147:1712–14. doi:10.1016/j.jtcvs.2014.01.012.
[17] Weinstein S, Bello R, Pizarro C, Fynn-Thompson F, Kirklin J, Guleserian K, et al. The use of the berlin heart EXCOR in patients with functional single ventricle. J Thorac Cardiovasc Surg 2014;147:697–704. doi:10.1016/j.jtcvs.2013.10.030.
[18] Halaweish I, Ohye RG, Si MS. Berlin heart ventricular assist device as a long-term bridge to transplantation in a Fontan patient with failing single ventricle. Pediatr Transplant 2015;19:E193–5. doi:10.1111/petr.12607.
[19] Rodefeld MD, Coats B, Fisher T, Giridharan GA, Chen J, Brown JW, et al. Cavopulmonary assist for the univentricular Fontan circulation: von Kármán viscous impeller pump (VIP ™). J Thorac Cardiovasc Surg 2010;140:529–36. doi:10.1016/j.jtcvs.2010.04.037.
[20] Bhavsar SS, Kapadia JY, Chopski SG, Throckmorton AL. Intravascular mechanical cavopulmonary assistance for patients with failing Fontan physiology. Artif Organs 2009;33:977–87. doi:10.1111/j.1525-1594.2009.00940.x.
[21] Throckmorton AL, Lopez-Isaza S, Downs EA, Chopski SG, Gangemi JJ, Moskowitz W. A viable therapeutic option: mechanical circulatory support of the failing Fontan physiology. Pediatr Cardiol 2013;34:1357–65. doi:10.1007/s00246-013-0649-9.
[22] Derk G, Laks H, Biniwale R, Patel S, De Lacruz K, Mazor E, et al. Novel techniques of mechanical circulatory support for the right heart and Fontan circulation. Int J Cardiol 2014;176:828–32. doi:10.1016/j.ijcard.2014.08.012.
[23] Gandolfo F, Brancaccio G, Donatiello S, Filippelli S, Perri G, Iannace E, et al. Mechanically assisted total cavopulmonary connection with an axial flow Pump: computational and in vivo study. Artif Organs 2016;40:43–9. doi:10.1111/aor.12641.
[24] Boni L, Sasaki T, Ferrier WT, Yeung JT, Reichenbach SH, Riemer RK, et al. Challenges in longer-term mechanical support of Fontan circulation in sheep. ASAIO J 2012;58:60–4. doi:10.1097/MAT.0b013e31823c0aa4.
[25] Jhun C-S, Newswanger RK, Cysyk J, Stauffer M, Weiss WJ, Rosenberg G. Fontan circulatory assist device. J. Med. Devices - Des. Med. Devices Conf. 2015;9:020924––3 Minneapolis, MN, USA: American Society of Mechanical Engineers. doi:10.1115/1.4030136.
[26] Chopski SG, Fox CS, McKenna KL, Riddle ML, Kafagy DH, Stevens RM, et al. Physics-driven impeller designs for a novel intravascular blood pump for patients with congenital heart disease. Med Eng Phys 2016;38:622–32. doi:10.1016/j.medengphy.2016.03.010.
[27] Giridharan GA, Koenig SC, Kennington J, Sobieski MA, Chen J, Frankel SH, et al. Performance evaluation of a pediatric viscous impeller pump for Fontan cavopulmonary assist. J Thorac Cardiovasc Surg 2013;145:249–57. doi:10.1016/j.jtcvs.2012.01.082.
[28] Haggerty CM, Fynn-Thompson F, McElhinney DB, Valente AM, Saikrishnan N, Del Nido PJ, et al. Experimental and numeric investigation of impella pumps as cavopulmonary assistance for a failing Fontan. J Thorac Cardiovasc Surg 2012;144:563–9. doi:10.1016/j.jtcvs.2011.12.063.
[29] Cysyk J, Clark JB, Newswanger R, Jhun C-S, Izer J, Finicle H, et al. Chronic in vivo test of a right heart replacement blood pump for failed Fontan circulation. ASAIO J 2018:1. doi:10.1097/MAT.0000000000000888. [Epub ahead of print].
[30] Timms D. A review of clinical ventricular assist devices. Med Eng Phys 2011;33:1041–7. doi:10.1016/j.medengphy.2011.04.010.
[31] Granegger M, Schweiger M, Schmid Daners M, Meboldt M, Hübler M. Cavopulmonary mechanical circulatory support in Fontan patients and the need for physiologic control: a computational study with a closed-loop exercise model. Int J Artif Organs 2018;41:261–8. doi:10.1177/0391398818762359.
[32] Kavarana MN, Jones JA, Stroud RE, Bradley SM, Ikonomidis JS, Mukherjee R. Pulmonary arteriovenous malformations after the superior cavopulmonary shunt: mechanisms and clinical implications. Expert Rev Cardiovasc Ther 2014;12:703–13. doi:10.1586/14779072.2014.912132.
[33] Ovroutski S, Nordmeyer S, Miera O, Ewert P, Klimes K, Kühne T, et al. Caval flow reflects Fontan hemodynamics: quantification by magnetic resonance imaging. Clin Res Cardiol 2012;101:133–8. doi:10.1007/s00392-011-0374-4.
[34] Sundareswaran KS, Reichenbach SH, Masterson KB, Butler KC, Farrar DJ. Low bearing wear in explanted heartmate II left ventricular assist devices after chronic clinical support. ASAIO J 2013;59:41–5. doi:10.1097/MAT.0b013e3182768cfb.
[35] Pfleiderer C, Petermann H. Strömungsmaschinen. 6th ed. Berlin: Springer-Verlag Berlin Heidelberg; 1991.
[36] Boes S, Thamsen B, Haas M, Schmid Daners M, Meboldt M, Granegger M. Hydraulic characterization of implantable rotary blood pumps. IEEE Trans Biomed Eng 2018;9294 1–1. doi:10.1109/TBME.2018.2876840.
[37] Hochareon P, Manning KB, Fontaine Aa, Tarbell JM, Deutsch S. Correlation of in vivo clot deposition with the flow characteristics in the 50 cc penn state artificial Heart: a preliminary study. ASAIO J 2004;50:537–42. doi:10.1097/01.MAT.0000145694.40637.A0.
[38] Goubergrits L, Affeld K. Numerical estimation of blood damage in artificial organs. Artif Organs 2004;28:499–507. doi:10.1111/j.1525-1594.2004.07265.x.
[39] Fraser KH, Taskin ME, Griffith BP, Wu ZJ. The use of computational fluid dynamics in the development of ventricular assist devices. Med Eng Phys 2011;33:263–80. doi:10.1016/j.medengphy.2010.10.014.

[40] Thamsen B, Mevert R, Lommel M, Preikschat P, Gaebler J, Krabatsch T, et al. A two-stage rotary blood pump design with potentially lower blood trauma: a computational study. Int J Artif Organs 2016;39:178–83. doi:10.5301/ijao.5000482.
[41] Ohuchi H, Yasuda K, Miyazaki A, Kitano M, Sakaguchi H, Yazaki S, et al. Haemodynamic characteristics before and after the onset of protein losing enteropathy in patients after the Fontan operation. Eur J Cardio-Thoracic Surg 2013;43:e49–57. doi:10.1093/ejcts/ezs714.
[42] CD-ADAPCO. STAR-CCM+ documentation 2014, https://documentation.thesteveportal.plm.automation.siemens.com/starccmplus_latest_en/; [Accessed 26 Jun 2019].
[43] Fiala D, Lomas KJ, Stohrer M. A computer model of human thermoregulation for a wide range of environmental conditions: the passive system. J Appl Physiol 1999;87:1957–72. doi:10.1152/jappl.1999.87.5.1957.
[44] Gieras JF, Koenig AC, Vanek LD. Calculation of eddy current losses in conductive sleeves of synchronous machines. In: Proceedings of the 18th IEEE international conference on electrical machines. IEEE; 2008. p. 1–4. doi:10.1109/ICELMACH.2008.4800129.
[45] Huang Y, Zhu J, Guo Y. Thermal analysis of high-speed SMC motor based on thermal network and 3-D FEA with rotational core loss included. IEEE Trans Magn 2009;45:4680–3. doi:10.1109/TMAG.2009.2023065.
[46] Tang E, Restrepo M, Haggerty CM, Mirabella L, Bethel J, Whitehead KK, et al. Geometric characterization of patient-specific total cavopulmonary connections and its relationship to hemodynamics. JACC Cardiovasc Imaging 2014;7:215–24. doi:10.1016/j.jcmg.2013.12.010.
[47] Bradley E, Hendrickson B, Daniels C. Fontan liver Disease: review of an emerging epidemic and management options. Curr Treat Options Cardiovasc Med 2015;17:51. doi:10.1007/s11936-015-0412-z.
[48] Rodefeld MD, Frankel SH, Giridharan GA. Cavopulmonary assist: (em)powering the univentricular Fontan circulation. Semin Thorac Cardiovasc Surg Pediatr Card Surg Annu 2011;14:45–54. doi:10.1053/j.pcsu.2011.01.015.
[49] Guyton A, Hall J. Cardiac output, venous return, and their regulation. Textbook on medical physiology. 11th ed. Philadelphia: Elsevier Saunders; 2006. p. 232–44.
[50] Thamsen B, Blümel B, Schaller J, Paschereit CO, Affeld K, Goubergrits L, et al. Numerical analysis of blood damage potential of the heartmate II and heartware HVAD rotary blood pumps. Artif Organs 2015;39:651–9. doi:10.1111/aor.12542.
[51] Mehra MR, Naka Y, Uriel N, Goldstein DJ, Cleveland JC, Colombo PC, et al. A fully magnetically levitated circulatory pump for advanced heart failure. N Engl J Med 2017;376:440–50. doi:10.1056/NEJMoa1610426.
[52] Alvarez J, Rao V. HeartMate 3-a “Step” in the right direction. J Thorac Dis 2017;9:E457–60. doi:10.21037/jtd.2017.04.39.
[53] Chiu W-C, Slepian MJ, Bluestein D. Thrombus formation patterns in the heartmate II ventricular assist Device: clinical observations can be predicted by numerical simulations. ASAIO J 2014;60:237–40. doi:10.1097/MAT.0000000000000034.
[54] Yang F, Kormos RL, Antaki JF. High-speed visualization of disturbed pathlines in axial flow ventricular assist device under pulsatile conditions. J Thorac Cardiovasc Surg 2015;150:938–44. doi:10.1016/j.jtcvs.2015.06.049.
[55] Mehra MR, Goldstein DJ, Uriel N, Cleveland JC, Yuzefpolskaya M, Salerno C, et al. Two-Year outcomes with a magnetically levitated cardiac pump in heart failure. N Engl J Med 2018;378:1386–95. doi:10.1056/NEJMoa1800866.
[56] Sigloch H. Strömungsmaschinen : Grundlagen und Anwendungen. 6th ed. Munich: Hanser; 2018.